18

Carbon Nanotubes

CONTENTS

Meyya Meyyappan
NASA Ames Research Center

Deepak Srivastava
NASA Ames Research Center

18.1 Introduction

Carbon nanotubes (CNT) were discovered by Iijima[1] as elongated fullerenes in 1991. Since then research on growth, characterization, and application development has exploded due to the unique electronic and extraordinary mechanical properties of CNTs. The CNT can be metallic or semiconducting and thus offers possibilities to create semiconductor–semiconductor and semiconductor–metal junctions useful in devices. The high tensile strength, Young's modulus, and other mechanical properties hold promise for high-strength composites for structural applications. Researchers have been exploring the potential of CNTs in a wide range of applications: nanoelectronics, sensors, field emission, displays, hydrogen storage, batteries, polymer matrix composites, body armor, reinforcement material, nanoscale reactors, and electrodes, to name a few. In this chapter, an overview of this rapidly emerging field is provided.

First, the structure of the nanotube and properties are explained. Unlike many other fields in science and engineering, the evolution of carbon nanotubes to its current level owes significantly to the contributions from modeling and simulation. Computational nanotechnology has played an early and major role in predicting as well as explaining the interesting properties of CNTs. Therefore, a section is devoted to modeling and simulation after the description of the properties. Then nanotube growth is covered in detail, followed by material development functions such as purification and characterization. Finally, a review of the current status of various applications is provided.

18.2 Structure and Properties of Carbon Nanotubes

A single-wall carbon nanotube (SWCNT) is best described as a rolled-up tubular shell of graphene sheet (Figure 18.1a) which is made of benzene-type hexagonal rings of carbon atoms.[2] The body of the tubular shell is thus mainly made of hexagonal rings (in a sheet) of carbon atoms, whereas the ends are capped by half-dome-shaped half-fullerene molecules. The natural curvature in the side-walls is due to the rolling of the sheet into the tubular structure, whereas the curvature in the end caps is due to the presence of topological (pentagonal rings) defects in the otherwise hexagonal structure of the underlying lattice. The role of a pentagonal ring defect is to give a positive (convex) curvature to the surface, which helps in closing the tube at the two ends. A multi-wall nanotube (MWCNT) is a rolled-up stack of graphene sheets into concentric SWCNTs, with the ends again either capped by half-fullerenes or kept open. A nomenclature (n,m), used to identify each single-wall nanotube, refers to integer indices of two graphene unit lattice vectors corresponding to the chiral vector of a nanotube.[2] Chiral vectors determine the directions along which the graphene sheets are rolled to form tubular shell structures and axis vectors perpendicular to the tube as explained in Reference 2. The nanotubes of type (n,n), as shown in Figure 18.1b, are commonly called armchair nanotubes because of the _/¯_/ shape, perpendicular to the tube

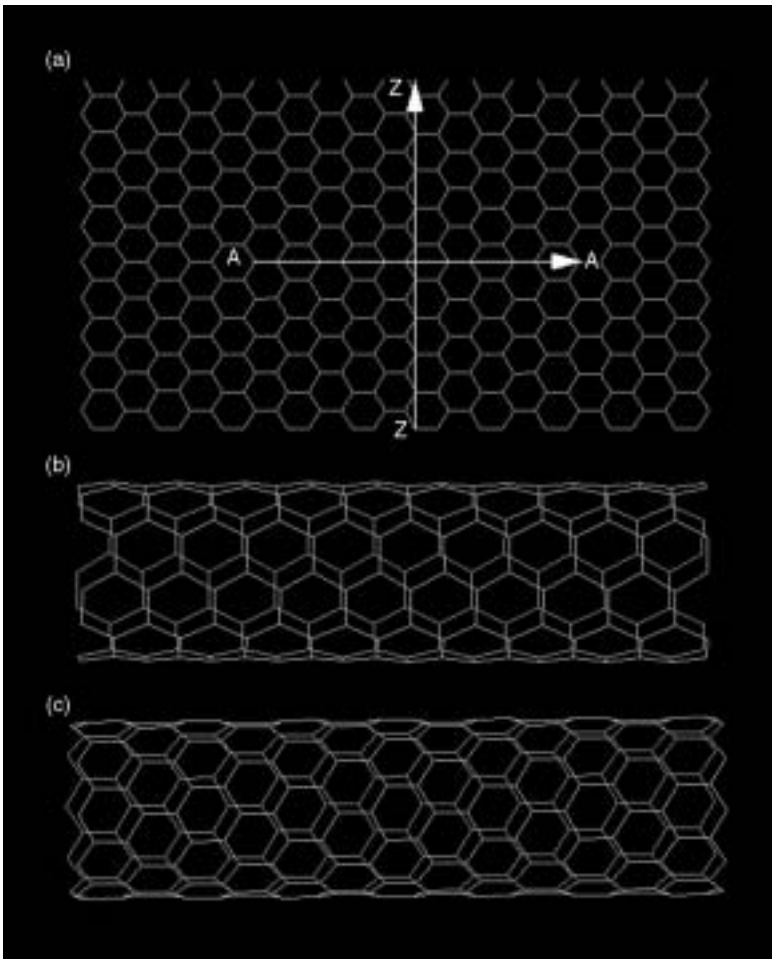

FIGURE 18.1 (a) A graphene sheet made of C atoms placed at the corners of hexagons forming the lattice with arrows AA and ZZ, denoting the rolling direction of the sheet to make (b) a (5,5) armchair nanotube and (c) a (10,0) zigzag nanotube.

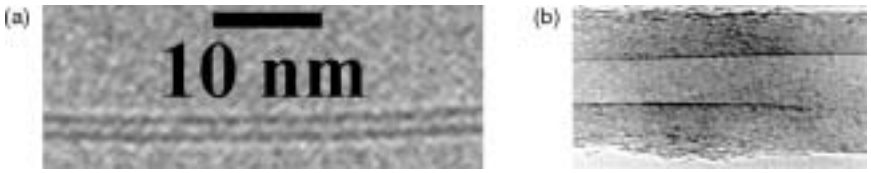

FIGURE 18.2 TEM images of (a) SWCNT and (b) MWCNT.

axis, and have a symmetry along the axis with a short unit cell (0.25 nm) that can be repeated to make the entire section of a long nanotube. Another type of nanotube (n,0) is known as zigzag nanotube (Figure 18.1c) because of the \/\/ shape perpendicular to the axis and as well as the short unit cell (0.43 nm) along the axis.[3] All the remaining nanotubes are known as chiral or helical nanotubes and have longer unit cell sizes along the tube axis. Transmission electron microscopy (TEM) images of an SWCNT and an MWCNT are shown in Figure 18.2. Details of the symmetry properties of the nanotubes of different chiralities are explained in detail in Reference 2.

The single- and multi-wall nanotubes are interesting nanoscale materials for several reasons. A single-wall nanotube can be either metallic or semiconducting, depending on its chiral vector (n,m), where n and m are two integers. A metallic nanotube is obtained when the difference n–m is a multiple of three. If the difference is not a multiple of three, a semiconducting nanotube is obtained. In addition, it is also possible to connect nanotubes with different chiralities creating nanotube heterojunctions, which can form a variety of nanoscale molecular electronic device components.

Single- and multi-wall nanotubes have very good elastomechanical properties because the two-dimensional arrangement of carbon atoms in a graphene sheet allows large out-of-plane distortions, while the strength of carbon–carbon in-plane bonds keeps the graphene sheet exceptionally strong against any in-plane distortion or fracture. These structural and material characteristics of nanotubes point toward their possible use in making the next generation of extremely lightweight but highly elastic and strong composite materials.

Nanotubes are high aspect–ratio structures with good electrical and mechanical properties. Consequently, the applications of nanotubes in field-emission displays, and scanning probe microscopic tips for metrology have begun to materialize in the commercial sector.

Because nanotubes are hollow, tubular, and caged molecules, they have been proposed as lightweight large-surface-area packing material for gas storage and hydrocarbon fuel storage devices, gas or liquid filtration devices, nanoscale containers for molecular drug delivery, and casting structures for making nanowires and nanocapsulates.

Carbon-based materials are ideally suitable as molecular-level building blocks for nanoscale systems design, fabrication, and applications. From a structural or functional materials perspective, carbon is the only element that exists in a variety of shapes and forms with varying physical and chemical properties. For example, diamond and layered graphite forms of carbon are well known, but the same carbon also exists in planar sheet, rolled-up tubular, helical spring, rectangular hollow box, and nanoconical forms. All basic shapes and forms needed to build any complex molecular-scale architectures, thus, are readily available with carbon. Additionally, by coating any carbon-based nanoscale devices with biological lipid layers and/or protein molecules, it may be possible to extend also into the rapidly expanding area of bionanotechnology.

18.3 Computational Modeling and Simulation

The structural, electronic, mechanical, and thermal properties of interacting, bulk, condensed-matter systems were studied in the earlier days with analytical approximation methods for infinite systems. Numerical simulations of the finite sample systems have become more common recently due to the availability of powerful computers. *Molecular dynamics* (MD) refers to an approach where the motion of atoms or molecules is treated in approximate finite difference equations of Newtonian mechanics. The

use of classical mechanics is well justified, except when dealing with very light atoms and very low temperatures. The dynamics of complex condensed-phase systems such as metals and semiconductors is described with explicit or implicit many-body force-field functions using Embedded Atom Method (EAM)-type potentials for metals[4] and Stillinger–Weber (SW)[5] and/or Tersoff–Brenner (T–B)[6,7]-type potentials for semiconductors.[8] The T–B-type potentials are parameterized and particularly suited for carbon-based systems (such as carbon nanotubes) and have been used in a wide variety of scenarios yielding results in agreement with experimental observations. However, currently, there is no universal classical force-field function that works for all materials and in all scenarios. Consequently, one needs to be careful where true chemical changes (involving electronic rearrangements) with large atomic displacements are expected to occur.

In its global structure, a general MD code typically implements an algorithm to find a numerical solution of a set of coupled first-order ordinary differential equations given by the Hamiltonian formulation of Newton's Second Law. The equations of motion are numerically integrated forward in finite time-steps using a predictor–corrector method. A major distinguishing feature of the Tersoff–Brenner potential[6,7] is that short-range bonded interactions are reactive so that chemical bonds can form and break during the course of a simulation. Therefore, compared with other molecular dynamics codes, the neighbor list describing the environment of each atom includes only a few atoms and needs to be updated more frequently. The computational cost of the many-body bonded interactions is relatively high compared with the cost of similar methods with nonreactive interactions with simpler functional forms. As a result, the overall computational costs of both short-range interactions and long-range, nonbonding van der Waals interactions are roughly comparable.

For large-scale atomistic modeling (10^5–10^8 atoms), multiple processors are used for MD simulations, and the MD code needs to be parallelized. A route to the parallelization of a standard MD code involves decoupling the neighbor list construction from the computation of the atomic forces and parallelizing each part in the most efficient way possible. Parallelization of the MD code using Tersoff–Brenner potential for carbon atom interactions was attempted and achieved recently. An example of the parallel implementation of this classical MD code is described in detail in Reference 9. This parallelized MD code has been utilized in simulations of mechanical properties of the nanotubes, nanotube–polymer composites, mechanical strain-driven chemistry of carbon nanotubes, and molecular gears and motors powered by laser fields.[3]

In recent years, several more accurate quantum molecular dynamics schemes have been developed in which the forces between atoms are computed at each time-step via quantum mechanical calculations within the Born–Oppenheimer approximation. The dynamic motion for ionic positions is still governed by Newtonian or Hamiltonian mechanics and described by molecular dynamics. The most widely known and accurate scheme is the Car–Parrinello (CP) molecular dynamic method,[10] where the electronic states and atomic forces are described using the *ab-initio* density functional method (usually within the local density approximation, LDA). In the intermediate regimes, the tight-binding molecular dynamics (TBMD)[11] approach for up to a few thousand atoms provides an important bridge between the *ab initio* quantum MD and classical MD methods. The computational efficiency of the tight-binding method derives from the fact that the quantum Hamiltonian of the system can be parameterized. Furthermore, the electronic structure information can be easily extracted from the tight-binding Hamiltonian, which in addition also contains the effects of angular forces in a natural way. In a generalized *nonorthogonal* TBMD scheme, Menon and Subbaswami have used a minimal number of adjustable parameters to develop a transferable scheme applicable to clusters as well as bulk systems containing Si, C, B, N, and H.[12,13] The main advantage of this approach is that it can be used to find an energy-minimized structure of a nanoscale system under consideration without symmetry constraints. The parallelization of the TBMD code involves parallelization of the direct diagonalization part of the electronic Hamiltonian matrix as well as that of the MD part. The parallelization of a sparse symmetric matrix giving many eigenvalues and eigenvectors is a complex step in the simulation of large intermediate-range systems and needs development of new algorithms.

Ab initio or first-principles method is an approach to solve complex quantum many-body Schroedinger equations using numerical algorithms.[14] The *ab initio* method provides a more accurate description of quantum mechanical behavior of materials properties even though the system size is currently limited to only a few hundred atoms. Current *ab initio* simulation methods are based on a rigorous mathematical foundation of the density functional theory (DFT).[15,16] This is derived from the fact that the ground-state total electronic energy is a function of the density of the system. For practical applications, the DFT–LDA method has been implemented with a pseudopotential approximation and a plane-wave (PW) basis expansion of single-electron wave functions.[14] These approximations reduce the electronic structure problem as a self-consistent matrix diagonalization problem. One of the popular DFT simulation programs is the Vienna *Ab initio* Simulation Package (VASP), which is available through a license agreement.[17]

In computational nanotechnology research, these three simulation methods can be used in a complementary manner to improve computational accuracy and efficiency. Based on experimental observations or theoretical dynamic and structure simulations, the atomic structure of a nanosystem can first be investigated. After the nanoscale system configurations are finalized, the electronic behaviors of the system are investigated through static *ab initio* electronic energy minimization schemes[14] or through studies of the quantum conductance[18] behavior of the system. This strategy has been covered in detail in a recent review article focusing on computational nanotechnology.[3]

In the following we describe several representative examples where computational nanotechnology has clearly played an important role in either explaining some recent experimental observations or predicting structures (or properties) that were later fabricated (or measured) in experiments.

18.3.1 Nanomechanics of Nanotubes and Composites

SWCNTs and MWCNTs have been shown to have exceptionally strong and stiff mechanical characteristics along the axis of the tube and very flexible characteristics along the axis of the tube.[19–21] For axial deformations, the Young's modulus of the SWCNTs can reach beyond 1 TPa, and the yield strength can be as large as 120 GPa. The initial investigations, using classical molecular dynamics simulations with Tersoff–Brenner potential, showed that the tubes are extremely stiff under axial compression and that the system remains within elastic limit even for very large deformations (up to 15% strain).[9,19] Nonlinear elastic instabilities, with the appearance of fin-like structures, are observed during these deformations; but the system remains within elastic limits and returns to the original unstrained state as soon as the external constraining forces are removed. As shown in Figure 18.3, when compressed beyond elastic limits, the single- and multi-wall nanotubes undergo sideway bucklings, and plastic deformations occur mainly through extreme bending situations in the sideway-buckled tubes. A significantly different deformation mode, however, was also predicted where the nanotube essentially remains straight, but the structure locally collapses at the location of the deformation[20] (Figure 18.4). This generally occurs for thin tubes and for tube lengths shorter than the Euler buckling limit. The local collapse is driven by graphitic to diamond-like bonding transition at the location of the collapse. Both of the simulated collapsing mechanisms have been observed in experiments.[22] The tensile strain, on the other hand, causes formation of Stone–Wales type topological defects in the tube (Figure 18.5), which leads to thinning and collapse of the tube when stretched further.[23–25] The yielding strains in all scenarios have been simulated in detail and show a strong dependence on the rate at which strain is applied as well as the temperature of the simulation system.[26] In agreement with recent experimental observations,[27] predictions show that at room temperature and at experimentally realizable strain rates, nanotubes typically yield at about 5–10% strain.[26]

Simulations of nanotube–polymer composites are currently in the preliminary stages. A few attempts have been made to characterize mechanical and thermal properties of CNT composite materials with molecular dynamics simulations. It is expected that the superior mechanical, thermal, and electrical characteristics of individual SWCNTs and MWCNTs in a polymer, ceramic, or metal matrix could be imparted to the resulting composite material as well. Several recent experiments on the preparation

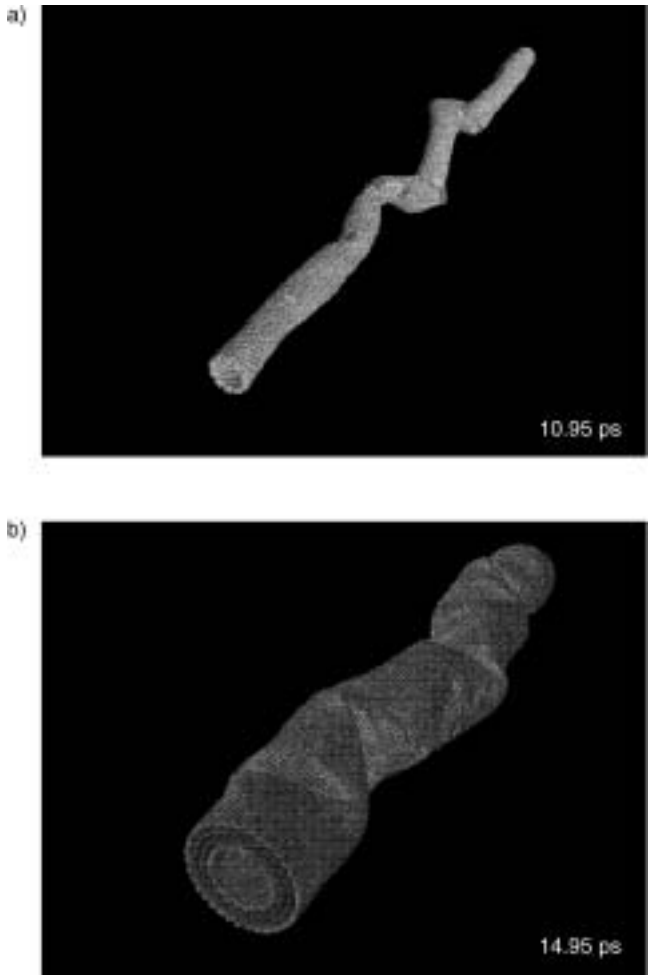

FIGURE 18.3 (a) An axially compressed single-wall nanotube within elastic limit shows sideways buckling and accumulation of strain at the tip of the sideways-buckled structure. (b) Same as in (a) except for a multi-wall nanotube with four walls.

and mechanical characterization of CNT–polymer composites have been reported.[27–31] In preliminary MD investigations of the nanotube–polymer composites above glass transition temperature, the thermal expansion coefficient of the composite matrix and diffusion coefficients of the polymer molecules increase significantly over their bare polymer matrix values. For example, the density vs. temperature profile of the polymer matrix and the composite material in Figure 18.6 shows a greater slope of the changes in density of the composite as compared with that in a bare polymer sample. The thermal expansion coefficient increases by as much as 40% by mixing of 5–10% of nanotubes in the polyethylene polymers.[32] The load transfer for axial straining of the polymer matrix composite is found to be driven by the difference in the Poisson ratio of the constituent materials. An SWCNT is typically a hard material and has a Poisson ratio of about 0.1 to 0.2, whereas polyethylene is a much softer polymeric material with a Poisson ratio of about 0.44. When the composite containing SWCNTs is under tensile strain, there is a resistance from the hard fibers to their surrounding matrix in response to the compression pressure driven by the tensile stress applied to the system. Thus the modulus of a composite can be enhanced with this mechanism even when there is not very good bonding between the SWCNT fibers and the polymer matrix. The Young's modulus is found to increase by as much as 30% for strain below the slippage limit.[32]

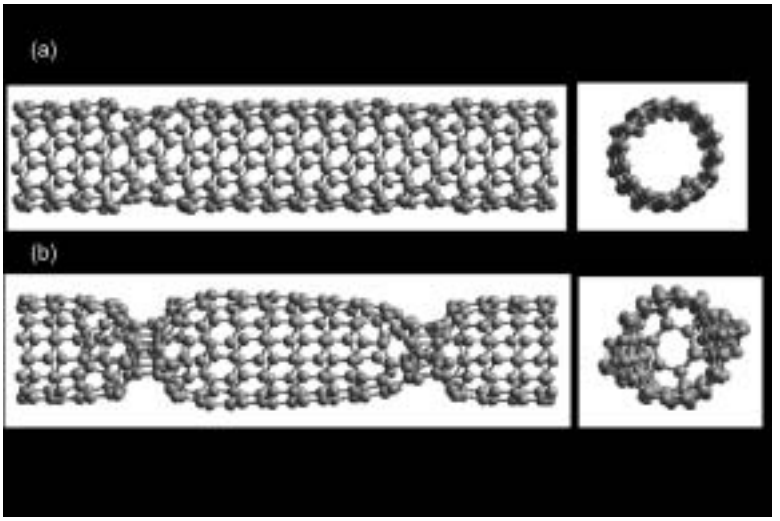

FIGURE 18.4 A 12% axially compressed (8,0) nanotube at (a) the beginning and (b) the end of a spontaneous local plastic collapse of the tube, which is driven by diamond-like bonding transitions at the location of the collapse. (b) Cross-sectional view.

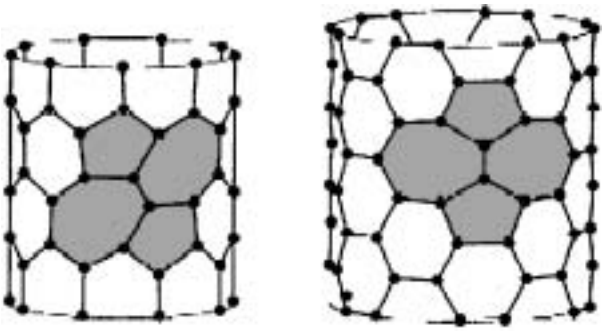

FIGURE 18.5 The Stone–Wales bond rotation on a zigzag and an armchair CNT, resulting in pentagon–heptagon pairs, can lengthen a nanotube, with the greatest lengthening for an armchair tube. (From P. Zhang and V. Crespi, *Phys. Rev. Lett.* 81, 5346, 1998. With permission.)

18.3.2 Molecular Electronics with Nanotube Junctions

The possibility of using carbon in place of silicon in the field of nanoelectronics has generated considerable enthusiasm. The metallic and semiconducting behavior as well as the electronic transport through individual single-wall nanotubes has been extensively investigated. The main thrust has been to see if the individual nanotube (or bundles of nanotubes) could be used as quantum molecular wires for interconnects in future computer systems. The ballistic electron transport through individual nanotubes has been supported by many independent studies, and it is considered to be one of the reasons that nanotubes exhibit high current density as compared with other materials at similar nanoscale.[33]

Inspired by the above, possibilities of connecting nanotubes of different diameter and chirality in nanotube heterojunctions as molecular electronic devices or switching components have also been investigated.[34] The simplest way is to introduce pairs of heptagon and pentagon in an otherwise perfect hexagonal lattice structure of the material. The resulting junction can act like a rectifying diode (Figure 18.7). Two terminal rectifying diodes were first postulated theoretically[34] and recently have been observed in experiments.[35]

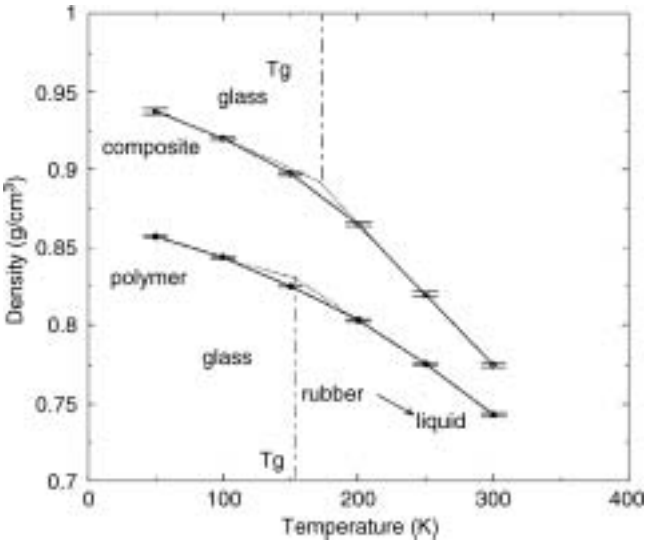

FIGURE 18.6 Density as a function of temperature for a polyethylene system (50 chains with $Np = 10$), and a CNT–polyethylene composite (2nm-long capped (10,0) CNT). The CNT composite has an increase of thermal expansion above T_g. From an MD simulation with van der Waals potential between CNT and matrix. Dihedral angle potential and torsion potential were used for the polyethylene matrix, and Tersoff–Brenner potential was used for carbon atom on the CNT.

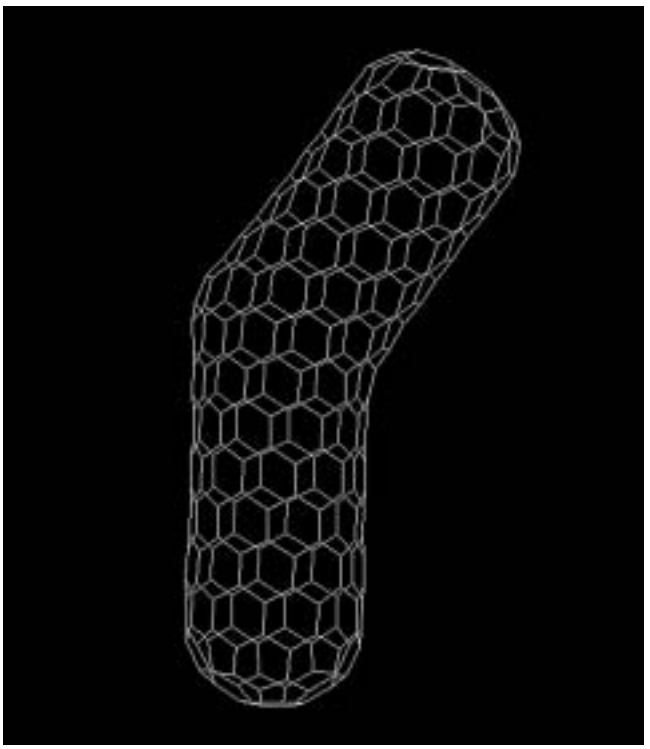

FIGURE 18.7 An example of two-terminal semiconducting (10,0)/(6,6) metallic nanotube junction that shows rectification behavior.

There are two ways to create heterojunctions with more than two terminals: first, connecting different nanotubes through topological defect mediated junctions;[36] second, laying down crossed nanotubes over each other and simply forming physically contacted or touching junctions.[37] The differences in the two approaches are the nature and characteristics of the junctions forming the device. In the first case, the nanotubes are chemically connected through bonding networks forming a stable junction that could possibly give rise to a variety of switching, logic, and transistor applications.[38] In the second case, the junction is merely through a physical contact and will be amenable to changes in the nature of the contact. The main applications in the second category will be in electromechanical bistable switches and sensors.[37] The bistable switches can act as bits in a CNT-based computing architecture.

Novel structures of carbon nanotube T- and Y-junctions have been proposed as models of three-terminal nanoscale monomolecular electronic devices.[36,39] The T-junctions can be considered as a specific case of a family of Y-junctions in which the two connecting nanotubes are perpendicular to each other (Figure 18.8). The pentagon–heptagon defect pair rule was found to be inapplicable in the

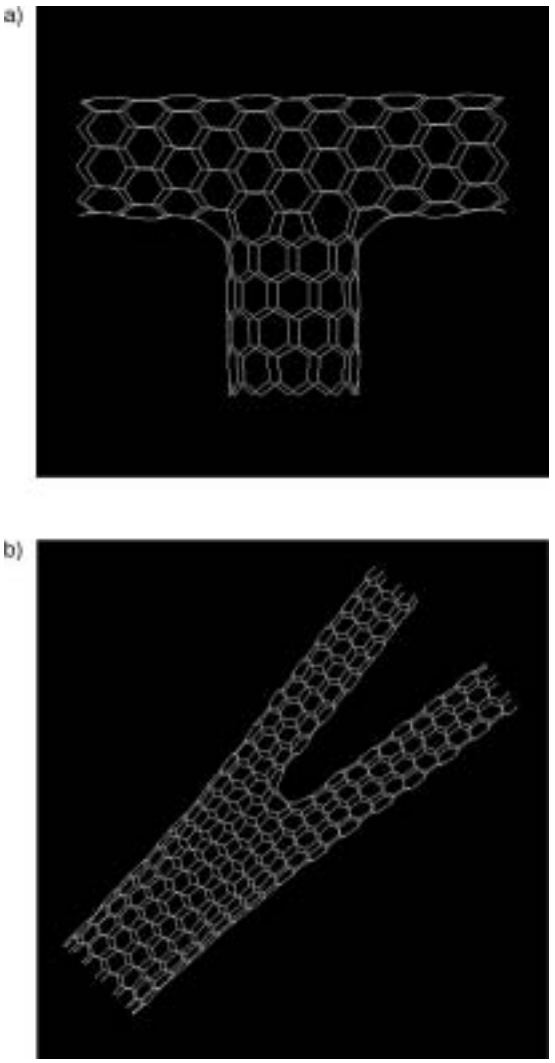

FIGURE 18.8 (a) An example of three-terminal carbon nanotube T-junction connecting metallic (9,0) and semiconducting (10,0) zigzag nanotubes. (b) An example of carbon nanotube Y-junction that is shown to exhibit rectification behavior as a two-terminal device, or a bistable switch and analog OR gate as a three-terminal device.

formation of the Y-junctions.[39] Recently, experimentalists have also succeeded in developing template-based chemical vapor deposition (CVD)[40] and pyrolysis of an organometallic precursor with nickelocene and thiophene[41] for the reproducible and high-yield fabrication of multi-wall carbon nanotube Y-junctions. The template-based method reports junctions consisting of large-diameter stems with two smaller branches that have an acute angle between them so they resemble tuning forks. The pyrolysis method reports multiple Y-junctions along a continuous multi-wall carbon nanotube. The electrical conductance measurements on these Y-junctions have been performed and show intrinsic nonlinear and asymmetric I-V behavior with rectification at room temperature. The quantum conductivity of a variety of carbon nanotube Y-junctions has also been calculated and shows current rectification under changes in the bias voltage.[42,43] The degree of rectification is found to depend on the type and nature of Y-junctions. Some junctions show good rectification while others show small leakage currents. The presence of rectification indicates, for the first time, the formation of a nanoscale molecular rectifying switch with a robust behavior that is reproducible in a high-yield fabrication method.[40,41] Moreover, simulations also show that the molecular switches thus produced can easily function as three-terminal bistable switches that are controlled by a control or *gate* voltage applied at a branch terminal.[42] Further, under certain biasing conditions, nanotube Y-junctions are shown to work as OR or XOR gates as well. The possible reasons for rectification in single-wall nanotube Y-junctions include constructive or destructive interference of the electronic wave functions through two different channels at the location of the junction; hence, the rectification is strongly influenced by the structural asymmetry across the two branches in a junction.[43]

In considering the architecture for future computing systems, we need not constrain ourselves to the specifications of the silicon-based devices, circuitry, and architecture. For example, a possible alternative architecture could be based on the structure and functioning of dendritic neurons in biological neural logic and computing systems. The tree shown in Figure 18.9 has a four-level branching structure and is made of 14 carbon nanotube Y-junctions. Such a structure is conceptually amenable to fabrication via a template-based CVD method, which is used for growing individual Y-junctions, and provides a first model of a biomimetic neural network made of single- or multi-wall carbon nanotubes.[3] In principle, such a *tree* could be trained to perform complex computing and switching applications in a single pass.

FIGURE 18.9 An illustration of a four-level dendritic neural tree made of 14 symmetric Y-junctions of the type in Figure 18.8.

18.3.3 Endofullerenes as Quantum Bits

The concept for quantum computation is based on quantum bits (qubits) which are the quantum state of a two-level system. A quantum computer with more than 20–30 qubits can outperform conventional classical computers for a certain class of computing tasks and will lead to a revolutionary increase in computing power.[44] Recent experimental demonstration of NMR quantum computation has already proven the feasibility of a device implementation of a real quantum computer.[45] However, these systems are limited in scaling up to a few qubits and would not be suitable as a platform to develop highly scalable quantum computers.

To overcome the scalability problem of NMR quantum computers, recently Kane proposed a solid-state quantum computer based on ^{31}P dopant atoms in bulk crystalline silicon.[46] In this proposal the nuclear spin of a ^{31}P atom is used as a solid-state qubit. The qubit state is controlled by hyperfine coupling to the weakly bound donor electron of the ^{31}P atom in Si lattice, and the quantum computer can be continuously scaled using microfabrication technology. However, the main challenge is that, experimentally, it is not known how to place a single dopant atom at a precise position in a silicon lattice and how to prevent the diffusion of the dopant atoms once placed in a desired position. A possible solution to these positioning and diffusion problems has been proposed using carbon-based nanotechnology.[47] In this new design, carbon diamond lattice is proposed to replace silicon diamond lattice as a host material for ^{31}P dopant atoms. This change of host materials solves both positioning and stability problem as follows.

The basic idea is to fabricate a diamond nanocrystallite with a ^{31}P dopant atom at the center using a bucky onion (multi-shell fullerenes). The sequence of fabrication steps for nanocrystallite is to first encapsulate a ^{31}P atom within a C_{60} fullerene via ion implantation methods to create an endofullerene, $\underline{P@C_{60}}$, as demonstrated in a recent experiment.[48] Second, use the $\underline{P@C_{60}}$ as a seed material to grow a bucky onion encapsulating the endofullerene; and third, use an e-beam or ion irradiation on the bucky onion to convert the inner core graphitic layers into a compressed diamond nanocrystallite.[49] Experiment has shown that the third step produces a compressed pristine diamond nanocrystallite with a 2 to 10 nm diameter.[49] Repeating the above fabrication steps with endofullerenes or doped bucky onions will lead to fabrication of doped diamond crystals.

The position control of ^{31}P atom qubits is conceptually feasible by fabricating arrays of 2 to 10 nm sized nanocrystallite (with ^{31}P at the center) qubits in any host dielectric material including diamond lattice. The stability of the dopant atom is ensured by much higher formation energies of vacancy (7 eV) and self-interstitial (~10 eV) defects in diamond than those in silicon lattice. The stability of the P atom is further enhanced by the stability of the P atom at substitutional site relative to interstitial site (by 15 eV). Because of higher formation energies, vacancy and self-interstitial defects are not likely to form during the graphite-to-diamond transformation process at the inner core of bucky onions; so the TED diffusion mechanism of ^{31}P atoms will be suppressed. Figure 18.10 shows the results of *ab initio* simulations of (a) $\underline{P@C_{60}}$ and (b) a ^{31}P doped at the center of a diamond nanocrystallite. The planar valence electron density (a) and the ^{31}P donor electron density in (111) plane in a diamond lattice (b) are shown in the two cases.[47] The spread of the donor electron density distribution, to define the donor electron mediated interaction between the neighboring qubits, has also been estimated.

18.3.4 Sensors and Actuators

As mentioned earlier, carbon nanotubes have different electronic properties depending on their chiral vectors, ranging from metals to semiconductors (1 eV bandgap). Semiconducting SWCNTs are very promising candidates for novel sensing applications because the surface modifications, due to chemical adsorption or mechanical deformation of the nanotubes, can directly modify the electronic conductance of nanotubes. Recent experimental and theoretical works have proved that SWCNTs are extremely sensitive to gas molecules,[50,51] and both chemical reactivity and electronic properties are strongly dependent on the mechanical deformation of nanotubes.[52,53] These characteristics have given rise to possibilities for use in chemical, vibration, and pressure sensor applications. The role of computational

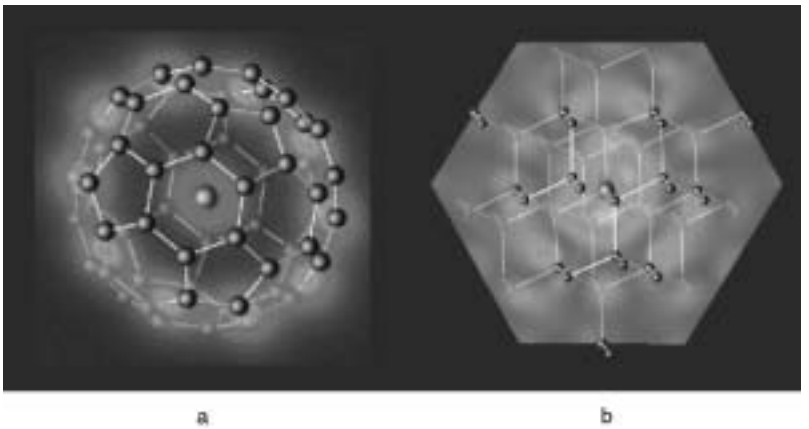

FIGURE 18.10 (a) The stable position and valance electron charge density of a P atom in a C_{60} fullerene. (b) The position and weakly bound donor electron density of the P atom after it has been encapsulated in a diamond nanocrystallite.

investigations in this case has been to precisely define how chemical reactivity[52] and electronic[53] properties change in a mechanically strained tube, and to determine the effect of gas-phase chemisorption[53] on the electronic characteristics of the system. It has been suggested that the mechanically tunable chemistry of nanotubes[52] will have possible applications in the chemisorption-induced electronics as well.[54] Experiments have shown that the nanotube sensors can detect ppm-level gas molecules at room temperature, and this opens a possibility of developing nanotube biosensors operating at room temperature.

For mechanical and vibration sensor applications, the full range of electronic bandgap changes as functions of axial compression, tensile stretch, torsion, and bending strain have been computed.[53] Additionally, as the cross-section of (8,0) SWCNT is flattened up to 40%, the bandgap of the nanotube decreases from 0.57 eV and disappears at 25% deformation. As the deformation further increases to 40%, the bandgap reopens and reaches 0.45 eV. This strong dependence of SWCNT band structure on the mechanical deformation can be applied to develop nanoscale mechanical sensors.[55]

18.3.5 Molecular Machines

The above examples provide a glimpse of a very broad field of applications and areas that are possible and directly fueled by the efforts and advances in computational nanotechnology. From materials to electronics, to computers and nanomachines, CNTs in fact could provide components of functional molecular-scale machines or robots (nanobots) in the future. Much of the recent progress in this field is in the experimental biomolecular motors arena, where significant understanding has been gained about how the natural biological motor systems work. Also, understanding has advanced in creating interfaces of nanoscale biomolecular motors with synthetic materials in solution-phase environments.[56] Means to power these machines through biomimetic physical and chemical phenomena are also under investigation. Ultimately, one can probably conceptualize nanoscale synthetic machines and motors that could be powered and controlled through external laser, electric, or magnetic fields and could operate in a chemical solution phase or inert gas environment. An example is the proposal of carbon nanotube-based gears[57] and how to power them through external laser fields.[58]

18.4 Nanotube Growth

The earliest approach to produce nanotubes was an arc process[59] as pioneered by Iijima.[1] This was soon followed by a laser ablation technique developed at Rice University.[60] In the last 5 years, chemical vapor

deposition (CVD) has become a common technique to grow nanotubes.[61–66] All these processes are described below. The figure of merit for an ideal growth process depends on the application. For development of composites and other structural applications, the expected metric is the ability to produce tons a day. In contrast, the ability to achieve controlled growth (of specified thickness) on patterns is important for applications in nanoelectronics, field emission, displays, and sensors. Even in these cases, such needs for patterned growth — undoubtedly originating from the microelectronics fabrication technology and knowledge base — may become irrelevant if circuits could be assembled from nanotubes in solution, as will be seen later in the section on applications. Regardless of the applications and growth approach, the ability to control the diameter and chirality of the nanotubes is critical to realize the promise of carbon nanotubes.

18.4.1 Arc Process and Laser Ablation

The arc process involves striking a DC arc discharge in an inert gas (such as argon or helium) between a set of graphite electrodes.[1,59] The electric arc vaporizes a hollow graphite anode packed with a mixture of a transition metal (such as Fe, Co, or Ni) and graphite powder. The inert gas flow is maintained at 50–600 Torr. Nominal conditions involve 2000 to 3000°C, 100 amps, and 20 volts. This produces SWCNTs in mixture of MWCNTs and soot. The gas pressure, flow rate, and metal concentration can be varied to change the yield of nanotubes; but these parameters do not seem to change the diameter distribution. Typical diameter distribution of SWCNTs by this process appears to be 0.7 to 2 nm.

In laser ablation, a target consisting of graphite mixed with a small amount of transition metal particles as catalyst is placed at the *end* of a quartz tube enclosed in a furnace.[60] The target is exposed to an argon ion laser beam that vaporizes graphite and nucleates carbon nanotubes in the shockwave just in front of the target. Argon flow through the reactor heated to about 1200°C by the furnace carries the vapor and nucleated nanotubes, which continue to grow. The nanotubes are deposited on the cooler walls of the quartz tube downstream from the furnace. This produces a high percentage of SWCNTs (~70%) with the rest being catalyst particles and soot.

18.4.2 Chemical Vapor Deposition (CVD)

CVD has been widely used in silicon integrated circuit (IC) manufacturing to grow a variety of metallic, semiconducting, and insulating thin films. Typical CVD relies on thermal generation of active radicals from a precursor gas, which leads to the deposition of the desired elemental or compound film on a substrate. Sometimes the same film can be grown at a much lower temperature by dissociating the precursor with the aid of highly energetic electrons in a glow discharge. In either case, catalysts are almost never required. In contrast, a transition metal catalyst is necessary to grow nanotubes from some form of hydrocarbon feedstock (CH_4, C_2H_2, C_2H_4…) or CO; and, in principle, extensive dissociation of the feedstock in the vapor phase is not necessary as the feedstock can dissociate on the catalyst surface. Nevertheless, this approach is still called CVD in the nanotube literature.

A thermal CVD reactor is simple and inexpensive to construct consisting of a quartz tube enclosed in a furnace. Typical laboratory reactors use a 1- or 2-inch quartz tube capable of holding small substrates. The substrate material may be Si, mica, quartz, or alumina. The setup needs a few mass flow controllers to meter the gases and a pressure transducer to measure the pressure. The growth may be carried out at atmospheric pressure or slightly reduced pressures using a hydrocarbon or CO feedstock. The growth temperature is in the range of 700 to 900°C. A theoretical study of CNT formation suggests that a high kinetic energy (and thus a high temperature, ≥ 900°C) and a limited, low supply of carbon are necessary to form SWCNTs.[67] Not surprisingly, CO and CH_4 are the two gases that have been reported to give SWCNTs. MWCNTs are grown using CO, CH_4, and other higher hydrocarbons at lower temperatures of 600 to 750°C. As mentioned earlier, CNT growth requires a transition metal catalyst. The type of catalyst, particle size, and the catalyst preparation techniques dictate the yield and quality of CNTs; this will be covered in more detail shortly.

As in silicon IC manufacturing, the carbon nanotube community has also looked to low-temperature plasma processing to grow nanotubes. The conventional wisdom in choosing plasma processing is that the precursor is dissociated by highly energetic electrons; and as a result, the substrate temperature can be substantially lower than in thermal CVD. However, this does not apply here because the surface-catalyzed nanotube growth needs at least 500°C; and it has not been established if a high degree of dissociation in the gas phase is needed. Nevertheless, several plasma-based growth techniques have been reported;[68–70] and in general, the plasma-grown nanotubes appear to be more vertically oriented than that possible by thermal CVD. This feature is attributed to the electric field in the plasma normal to the substrate. Because the plasma is very efficient in tearing apart the precursors and creating radicals, it is also hard to control and to keep the supply of carbon low to the catalyst particles. Hence, plasma-based growth always results in MWCNTs and filaments.

The plasma reactor consists of a high vacuum chamber to hold the substrate, mass flow controllers, a mechanical (roughing) pump and, if necessary, a turbopump (plasma reactors almost always run at reduced pressure, 0.1 to 50 Torr), pressure gauges, and a discharge source. The latter is the heart of the plasma-processing apparatus; and in CNT growth, microwave sources are widely used, probably because of the popularity of this source in the diamond community. The microwave system consists of a power supply at 2.45 GHz and wave guides coupled to the stainless steel growth chamber. Though the plasma can provide intense heating of the substrate, it is normal to have an independent heater for the substrate holder. Other plasma sources include inductive source and hot filament DC discharge. The latter uses a tungsten, tungsten carbide, or similar filament heated to about 2500 K with the gas flow maintained at 1 to 20 Torr. Simple DC or RF discharges can also be used in nanotube growth. These consist of two parallel-plate electrodes with one grounded and the other connected to either a DC or a 13.56 MHz power supply.

18.4.3 Catalyst Preparation

Several reported catalyst preparation techniques in the literature consist of some form of solution-based catalysts. One recipe for growing MWCNTs is as follows.[63] First, 0.5 g (0.09 mmol) of Pluronic P-123 triblock copolymer is dissolved in 15 cc of a 2:1 mixture of ethanol and methanol. Next, $SiCl_4$ (0.85 cc, 7.5 mmol) is slowly added using a syringe into the triblock copolymer/alcohol solution and stirred for 30 minutes at room temperature. Stock solutions of $AlCl \bullet 6H_2O$, $CoCl_2 \bullet 6H_2O$, and $Fe(NO_3)_3 \bullet 6H_2O$ are prepared at the concentration of the structure-directing agent (SDA) and inorganic salts. The catalyst solutions are filtered through 0.45 μm polytetrafluoroethylene membranes before being applied to the substrate. The substrate with the catalyst formulation is loaded into a furnace and heated at 700°C for 4 hours in air to render the catalyst active by the decomposition of the inorganic salts and removal of the SDA. Figure 18.11 shows SEM images of MWCNTs grown using this formulation in a thermal CVD reactor. A nanotube tower with millions of multi-walled tubes supporting each other by van der Waals force is seen. If the catalyst solution forms a ring during annealing, then a hollow tower results.

Several variations of solution-based techniques have been reported in the literature. All of them have done remarkably well in growing carbon nanotubes. A common problem with the above approaches is that it is difficult to confine the catalyst from solutions within small patterns. Another problem is the excessive time required to prepare the catalyst. A typical solution-based technique for catalyst preparation involves several steps lasting hours. In contrast, physical processes such as sputtering and e-beam deposition not only can deal with very small patterns but are also quick and simple in practice.[66,68,69] Delzeit et al. reported catalyst preparation using ion beam sputtering wherein an underlayer of Al (~10 nm) is deposited first, followed by 1 nm of Fe active catalyst layer.[66] Figure 18.12 shows SWCNTs grown by thermal CVD on a 400-mesh TEM grid used to pattern the substrate. Methane feedstock at 900°C was used to produce these nanotubes. The same catalyst formulation at 750°C with ethylene as the source gas yielded MWCNT towers.

One of the most successful approaches to obtain oriented arrays of nanotubes uses a nanochannel alumina template for catalyst patterning.[71] First, aluminum is anodized on a substrate such as Si or quartz, which provides ordered, vertical pores. Anodizing conditions are varied to tailor the pore diameter, height, and spacing between pores. This is followed by electrochemical deposition of a cobalt catalyst at the bottom of the pores. The catalyst is activated by reduction at 600°C for 4 to 5 hours. Figure 18.13 shows

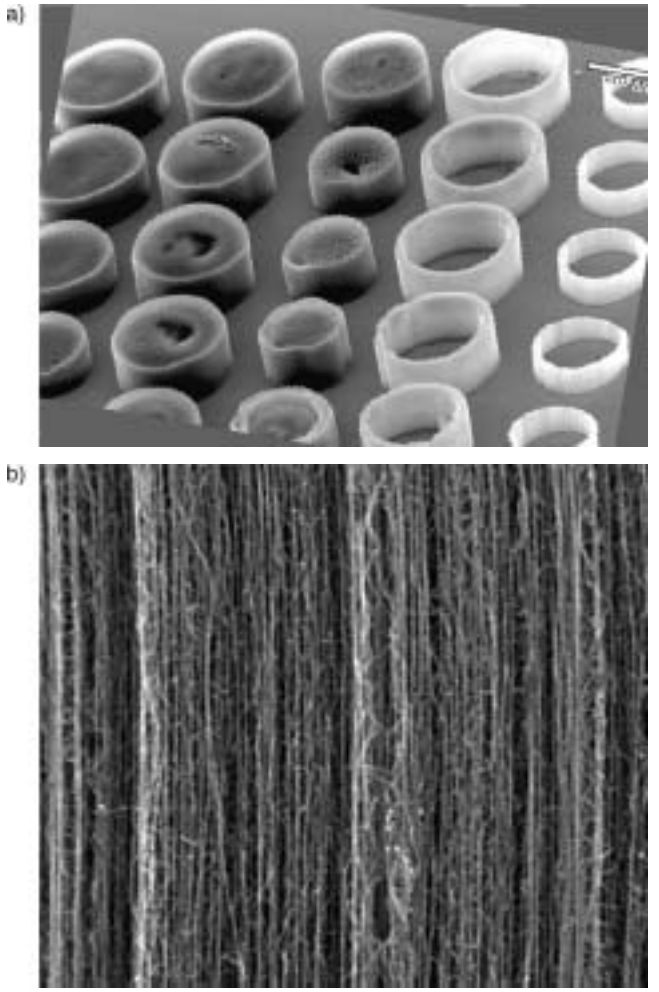

FIGURE 18.11 Multi-wall nanotubes grown by thermal CVD. (a) Different catalyst solution concentrations result in towers and ring-like structures. (b) Close-up view of one of these structures showing a forest of nanotubes supporting each other by van der Waals force, thus resulting in a vertical structure.

an ordered array of MWCNTs (mean diameter 47 nm) grown by CVD from 10% acetylene in nitrogen. The use of a template provides uniformity and vertically oriented nanotubes.

18.4.4 Continuous, High-Throughput Processes

The nanotube growth on substrates is driven by the desire to develop devices. Instead of supported catalysts, nanotubes have also been produced using catalysts floating in the gas phase. This approach is designed for production of large quantities of nanotubes in a continuous process. The earliest report[72] of such a process involved pyrolysis of a mixture containing benzene and a metallocene (such as ferrocene, cobaltocene, or nickelocene). In the absence of metallocene, only nanospheres of carbon were seen, but a small amount of ferrocene yielded large quantities of nanotubes. The growth system uses a two-stage furnace wherein a carrier gas picks up the metallocene vapor at around 200°C in the first stage, and the decomposition of the metallocene as well as pyrolysis of the hydrocarbon and catalytic reactions occur in the second stage at elevated temperatures (> 900°C). Acetylene with ferrocene or iron pentacarbonyl at 1100°C has been shown to yield SWCNTs in a continuous process in the same two-stage system. Andrews et al. also reported a continuous process for multiwall tubes using a ferrocyne–xylene mixture at temperatures as low as 650°C.[73]

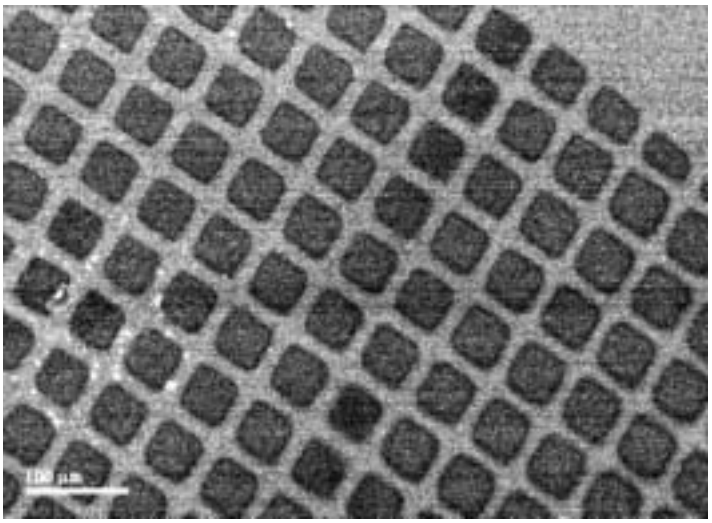

FIGURE 18.12 SWCNTs grown by thermal CVD on a 400-mesh TEM grid to pattern a silicon substrate.

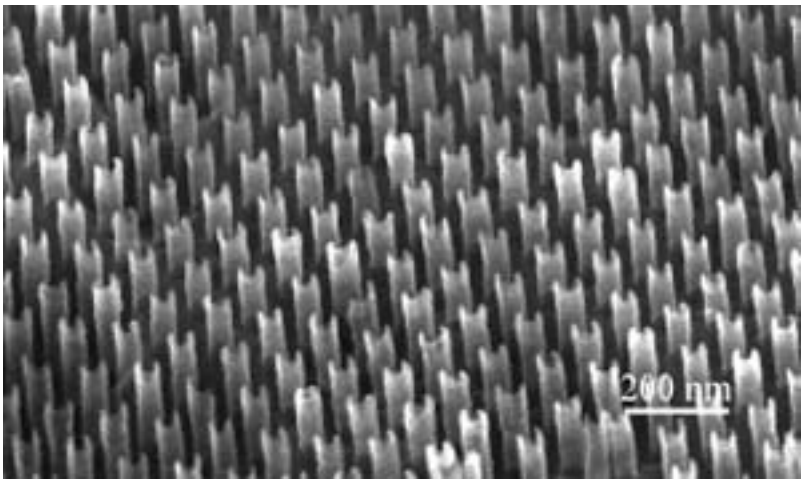

FIGURE 18.13 An ordered array of MWCNTs grown using an alumina template. (From J. Li, C. Papadopoulos, J.M. Xu, and M. Moskovits, *Appl. Phys. Lett.* 75, 367, 1999. With permission.)

Recently, a high-pressure process using CO (HiPCO) has been reported.[74] In this process, the catalyst is generated *in situ* by thermal decomposition of iron pentacarbonyl. The products of this decomposition include iron clusters in the gas phase that act as nuclei for the growth of SWCNTs using CO. The process is operated at pressures of 10 to 50 atm. and temperatures of 800 to 1200°C. SWCNTs as small as 0.7 nm in diameter are produced by this process. The current production rate is about 0.5 g/h, and the process seems to be amenable for scale-up for commercial production.

18.5 Material Development

18.5.1 Purification

The as-grown material typically contains a mixture of SWCNTs, MWCNTs, amorphous carbon, and catalyst metal particles; and the ratio of the constituents varies from process to process and depends on

growth conditions for a given process. Purification processes have been developed to remove all the unwanted constituents.[75] The purpose is to remove all the unwanted material and obtain the highest yield of nanotubes with no damage to the tubes. A typical process used in Reference 76 to purify Hipco-derived SWCNTs[74] is as follows. First, a sample of 50 mg is transferred to a 50 ml flask with 25 ml of concentrated HCl and 10 ml of concentrated HNO_3. The solution is heated for 3 hours and constantly stirred with a magnetic stirrer in a reflux apparatus equipped with a water-cooled condenser. This is done to remove iron and graphite nanocrystallites. The resulting suspension is transferred into centrifuge tubes and spun at 3220 g for 30 minutes. After pouring off the supernatant, the solid is resuspended and spun (30 minutes) three times in deionized water. Next, the solid is treated with NaOH (0.01 M) and centrifuged for 30 minutes. This process yields nanotube bundles with tube ends capped by half fullerenes. Finally, the sample is dried overnight in a vacuum oven at 60°C.

18.5.2 Characterization

High-resolution TEM is used (as in Figure 18.2) to obtain valuable information about the nanotube structure such as diameter, open vs. closed ends, presence of amorphous material, defects, and nanotube quality. In MWCNTs, the spacing between layers is 0.34 nm and, therefore, a count of the number of walls readily provides the diameter of the structure. Because the nature of catalyst and particle size distribution appear to be critical in determining the nanotube growth characteristics, researchers have used TEM, EDX, and AFM to characterize the catalyst surface prior to loading in the growth reactor. These techniques together provide information on the particle size and chemical composition of the surface.[66]

Besides TEM, Raman scattering is perhaps the most widely used characterization technique to study nanotubes.[77–80] Raman spectroscopy of the SWCNTs is a resonant process associated with optical transition between spikes in the 1-d electronic density of states. Both the diameter and the metallic vs. semiconducting nature of the SWCNTs dictate the energy of the allowed optical transitions and, hence, this characteristic is used to determine the diameter and nature of the nanotubes. An example from Reference 66 is presented in Figure 18.14. The spectra was obtained in the back-scattering configuration using a 2 mW laser power (633 nm excitation) on the sample with a 1 μm focus spot. The nanotube G band zone is formed through graphite Brilliouin zone folding. The spectrum in Figure 18.14 shows the characteristic narrow G band at 1590 cm^{-1} and signature band at 1730 cm^{-1} for SWCNTs. A strong enhancement in the low frequency is also observed in the low-frequency region for the radial breathing mode (RBM). As shown in Reference 77, 1-d density of state of metallic nanotubes near the Fermi level has the first singularily bandgap between 1.7 and 2.2 eV, which will be resonant with 633 nm (1.96 eV) excitation line to the RBM. Using $\alpha = 248\ cm^{-1}$ in $\Omega_{RBM} = \alpha/d$, a diameter distribution of 1.14 to 2 nm

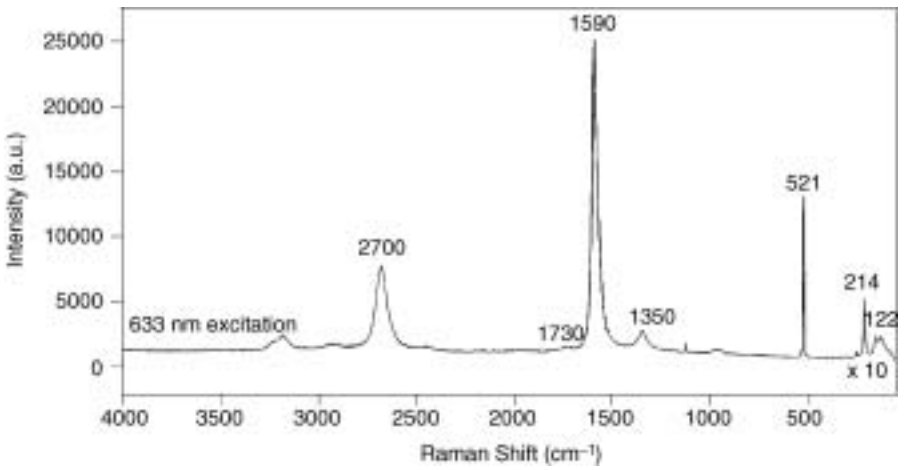

FIGURE 18.14 Raman spectra of CVD-grown SWCNT sample.

is computed for the sample in Figure 18.14, with the dominant distribution around 1.16 nm. The strong enhancement in 633 nm excitation[78] indicates that this sample largely consists of metallic nanotubes.

18.5.3 Functionalization

Functionalization of nanotubes with other chemical groups on the side-wall is attempted to modify the properties required for an application in hand. For example, chemical modification of the side-walls may improve the adhesion characteristics of nanotubes in a host polymer matrix to make functional composites. Functionalization of the nanotube ends can lead to useful chemical and biosensors.

Chen et al.[81] reported that reaction of soluble SWCNTs with dichlorocarbene led to the functionalization of nanotubes with Cl on the side-walls. The saturation of 2% of the carbon atoms in SWCNTs with C–Cl is sufficient to result in dramatic changes in the electronic band structure. Michelson et al.[82] reported fluorination of SWCNTs with F_2 gas flow at temperatures of 250 to 600°C for 5 hours. The fluorine is shown to attach covalently to the side-wall of the nanotubes. Two-point probe measurements showed that the resistance of the fluorinated sample increased to ~20 M Ω from ~15 Ω for the untreated material. While most functionalization experiments use a wet chemical or exposure to high-temperature vapors or gases, Khare et al.[76] reported a low-temperature, cold-plasma-based approach to attach functional groups to the nanotubes. They have been able to show functionalization with atomic hydrogen from an H_2 discharge as evidenced by the C–H stretching modes observed in the FTIR analysis of the samples. They also used a deuterium discharge to functionalize SWCNTs with D and showed C–D stretching modes in the region of 1940 to 2450 cm^{-1}.

18.6 Application Development

18.6.1 CNTs in Microscopy

Atomic-force microscopes (AFM) are widely used now by the research community to image and characterize various surfaces and also by the IC industry as a metrology tool. A typical AFM probe consists of a silicon or silicon–nitride cantilever with a pyramidal-shaped tip. This tip now can be made as small as 10 to 20 nm, offering reasonable resolution. However, the large cone angle of this tip (30 to 35°) makes it difficult for probing narrow and deep features such as trenches in IC manufacturing. Another serious drawback is that the tip is brittle, thus limiting its use in applications; either the tip breaks after only a limited use or it becomes blunt. For these reasons, a CNT probe has become an attractive alternative. Though early CNT probes[83,84] were manually attached to the tip of the AFM cantilever, currently it is possible to directly grow an SWCNT or MWCNT probe by CVD.[85,86] The CNT probe not only offers extraordinary nanometer-scale resolution but is also robust, due to its high strength and the ability to retain structural integrity even after deformation within elastic limit. Figure 18.15 shows an SWCNT probe prepared by CVD with diameter of ~2 nm. In a well-characterized CVD process, it may be possible to control the length of the probe by selecting the growth time. In the absence of knowledge of growth vs. time, it is possible to shorten the tip to the desired length by the application of an electric field to etch away the nanotube. Figure 18.16 shows a line/shape pattern of a polymeric photoresist on a silicon substrate. The image, obtained using a conventional silicon pyramidal tip (not shown here), shows sloping sides for the photoresist, which is an artifact due to the pyramidal shape of the tip. The image in Figure 18.16 was obtained using a MWCNT probe, which shows no such artifact but the vertical walls for the photoresist lines as confirmed by SEM.

In addition to profilometry, CNT tips are also useful in imaging thin films in semiconductor metrology. For example, Figure 18.17 shows an AFM image of a 2 nm film of Ir on mica surface collected with an SWCNT probe (~2 nm tip diameter). This affords a very high lateral resolution with grain sizes as small as 4 to 7 nm. Interestingly, even after continuous scanning for hours, the tip exhibits no detectable degradation in the lateral resolution of the grains. In contrast, the resolution capability becomes worse with time in the case of the silicon probe. As characterization tools in the IC industry, CNT probes would

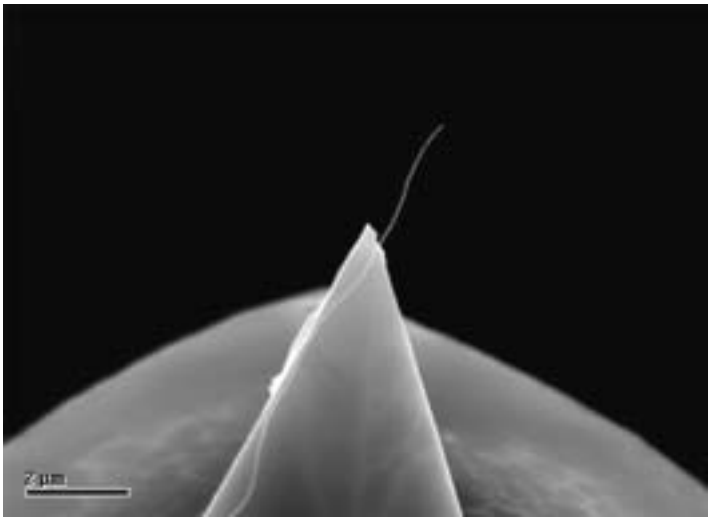

FIGURE 18.15 SWCMT tip grown by CVD at the end of an AFM cantilever.

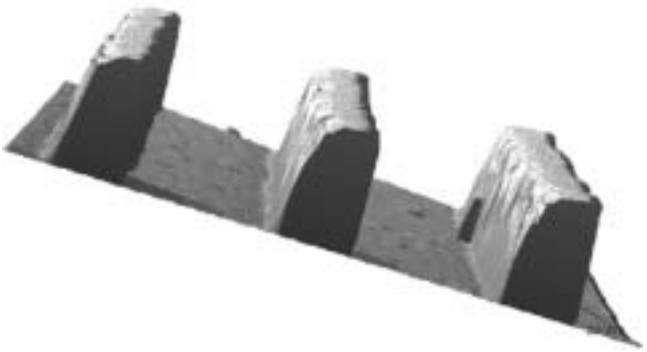

FIGURE 18.16 AFM profile of a 280 nm line/space photoresist pattern.

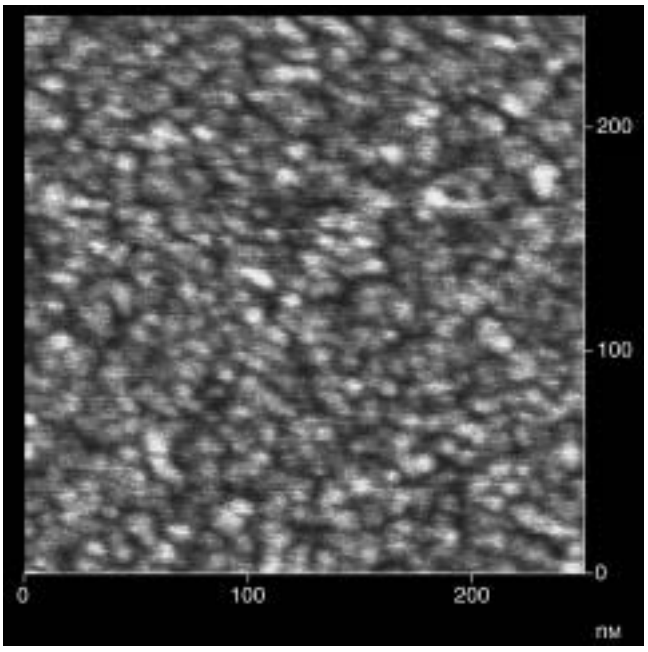

FIGURE 18.17 AFM image of a 2 nm Ir surface collected using an SWCNT tip.

require less frequent changing of probes, thus offering higher throughput. Researchers have also successfully used CNT probes to image biological samples.[83,85]

18.6.2 CNT-Based Nanoelectronics

The unique electronic properties of CNTs and possible devices from theoretical perspectives were discussed in detail in Sections 18.2 and 18.3. Room temperature demonstration of conventional switching mechanisms such as in field-effect transistors first appeared in 1998.[87,88] As shown in Figure 18.18, an SWCNT is placed to bridge a pair of metal electrodes serving as source and drain. The electrodes are defined using lithography on a layer of SiO_2 in a silicon wafer, which acts as the back gate. The variation of drain current with gate voltage at various source–drain biases for a 1.6 nm nanotube[87,88] clearly demonstrate that the gate can strongly control the current flow through the nanotube. In this device, the holes are the majority carriers of current as evidenced by an increase in current at negative gate voltages. Reference 89 provides a theoretical analysis of how the nanotube FETs work and shows that the electrode–nanotube contact influences the subthreshold channel conductance vs. gate voltage.

Since the pioneering demonstration of nanotube FETs, CNT logic circuits have been successfully fabricated. Figure 18.19 shows a CNT-based field-effect inverter consisting of n-type and p-type transistors.[90] The nanotube is grown using CVD between the source and the drain and on top of an SiO_2 layer with a silicon back gate. The as-grown nanotube exhibits p-type doping. Masking a portion of the nanotube and doping the remaining part with potassium vapor creates an n-type transistor. Combining the p- and the n-type transistors, complementary inverters are created. Applying a 2.9 V bias to the V_{DD}

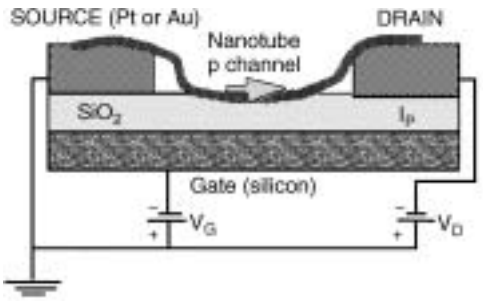

FIGURE 18.18 A carbon nanotube field-effect transistor.

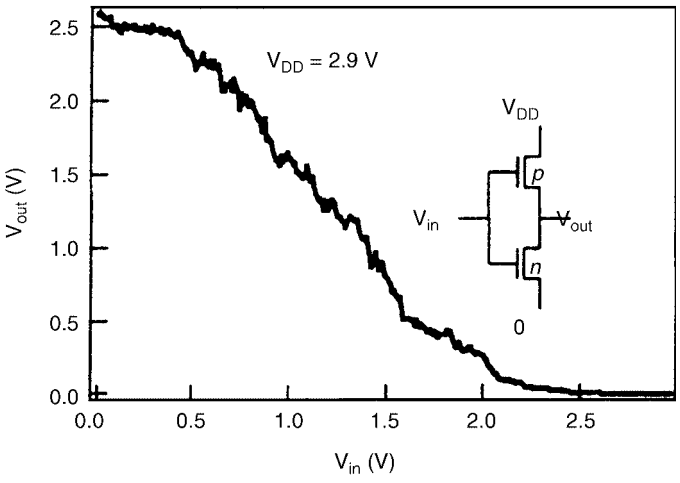

FIGURE 18.19 A carbon nanotube-based inverter.

terminal in the circuit and sweeping the gate voltage from 0 to 2.5 V yields an output voltage going from 2.5 V to 0. The inverter in Figure 18.19 shows a gain of 1.7 but does not exhibit an ideal behavior because, in this early demonstration, the PMOS is suspected to be leaky. Bachtold et al.[91] reported logic circuits with CNT transistors which show high gain (> 10), a large on–off ratio (> 10^5), and room temperature operation. Their demonstration included operations such as an inverter, a logic NOR, a static random-access memory cell, and an AC ring oscillator.

Fabrication of nanotube-based three-terminal devices involves horizontally placing nanotubes between the metal electrodes. While earlier demonstrations carefully transplanted a simple nanotube from bulk material, recent works have used CVD to bridge the electrodes with a nanotube.[90,92] This is indeed anything but routine as growth naturally occurs vertically from a surface. In this regard, successful fabrication of CNT Y-junctions (discussed in detail in Section 18.3) has been reported.[40,41] The I-V measurements on these CVD-grown multi-wall Y-tubes show reproducible rectification at room temperature. Alternatively, a concept proposed by Rueckes et al.[37] plans to use directed assembly of nanotubes from solution. This approach involves a suspended, crossed nanotube geometry that leads to bistable, electrostatically switchable ON/OFF states. Construction of nonvolatile random-access memory and logic functions using this approach is expected to reach a level of 10^{12} elements/cm^2.

18.6.3 Sensors

Significant research is in progress to develop CNT-based chemical, biological, and physical sensors. These efforts can be broadly classified into two categories: one that utilizes certain properties of the nanotube (such as a change in conductivity with gas adsorption) and the second that relies on the ability to functionalize the nanotube (tip and/or side-wall) with molecular groups that serve as sensing elements.

Gas sensors dedicated to sensing NO_2, NH_3, etc. use semiconducting metal oxides (SnO_2 for example) and conducting polymers. Most oxide-based sensors work at temperatures above 200°C but exhibit good sensitivity. Kong et al.[50] reported that the room temperature conductivity of CNTs changes significantly with exposure to NH_3 and NO_2, a property useful for developing sensors. Current–voltage characteristics of a 1.8 nm SWCNT placed between a pair of Ni/Au electrodes were studied before and after exposure to various doses of NH_3 and NO_2. The SWCNT samples used in the experiments were hole-doped semiconductors. Ammonia shifts the valence band of the CNT from the Fermi level and thus reduces the conductance due to hole depletion. The conductance was observed to decrease by a factor of 100 upon exposure to 1% NH_3. The response time, which may be defined as the time needed to see one order of magnitude change in conductance, was 1 to 2 minutes. The sensitivity, defined as the ratio of resistances before and after gas exposure, was 10 to 100. These results at room temperature compare favorably with metal oxides operating at 300 to 500°C.

To study the effect of NO_2, the device was operated with a gate voltage of 4 V at the back gate in a configuration discussed in Figure 18.18 under nanoelectronics (Section 18.6.2). This initially depletes the nanotubes, and exposure to NO_2 shifts the valence band closer to the Fermi level, thus increasing the holes in the nanotubes and conductance. The results for NO_2 are also encouraging. The conductance increase was about 1000 in response to 200 ppm NO_2, and the response time was 2 to 10 seconds. The sensitivity at room temperature was found to be 100 to 1000. One current drawback for deploying CNTs in sensors is the slow recovery of the CNTs to the initial state. In the above experiments, it took up to 12 hours for the conductivity of the CNTs to return to the original value after the source gas was withdrawn. Heating the sensor to 200°C reduced this period to about an hour. Similar large conductance changes upon exposure to oxygen have also been reported.[93] Work on functional sensors using nanotubes is rather limited. Xu[94] proposes IR detection using an ordered CNT array in a broad wavelength range of 1 to 15 μm.

18.6.4 Field Emission

The geometric properties of nanotubes, such as the high aspect ratio and small tip radius of curvature, coupled with the extraordinary mechanical strength and chemical stability, make them an ideal candidate

for electron field emitters. CNT field emitters have several industrial and research applications: flat panel displays, outdoor displays, traffic signals, and electron microscopy. De Heer et al.[95] demonstrated the earliest high-intensity electron gun based on field emission from a film of nanotubes. A current density of 0.1 mA/cm^2 was observed for voltages as low as 200 V. For comparison, most conventional field emitter displays operate at 300 to 5000 V, whereas cathode ray tubes use 30000 V. Since this early result, several groups have studied the emission characteristics of SWCNTs and MWCNTs.[96–100]

A typical field emission test apparatus consists of a cathode and anode enclosed in an evacuated cell at a vacuum of 10^{-9} to 10^{-8} Torr. The cathode consists of a glass or PTFE (polytetrafluoroethylene) substrate with metal-patterned lines, where a film of nanotubes can be transplanted after the arc-grown or laser oven material is purified. Instead nanotubes can be directly grown on the cathode in a CVD or plasma CVD chamber described earlier. The anode operating at positive potentials is placed at a distance of 20 to 500 μm from the cathode. The turn-on field, arbitrarily defined as the electric field required for generating 1 nA, can be as small as 1.5 V/μm. The threshold field — the electric field needed to yield a current density of 10 mA/cm^2 — is in the range of 5 to 8 V/μm. At low emission levels, the emission behavior follows the Fowler–Nordheim relation, i.e., the plot of ln (I/V^2) vs. ln (1/V) is linear. The emission current significantly deviates from the F–N behavior in the high field region and, indeed, emission current typically saturates. While most works report current densities of 0.1 to 100 mA/cm^2, very high current densities of up to 4 A/cm^2 have been reported by Zhu et al.[99]

Working full-color flat panel displays (FPD) and CRT lighting elements have been demonstrated by groups from Japan and Korea.[97,100] In the case of FPD, the anode structure consists of a glass substrate with phosphor-coated indium tin–oxide stripes. The anode and cathode are positioned perpendicular to each other to form pixels at their intersections. Appropriate phosphors such as Y_2O_2S: Eu, ZnS: Cu, Al, and ZnS: Ag, Cl are used at the anode for red, green, and blue colors, respectively. A 4.5 inch display showed a uniform and stable image over the entire 4.5 inch panel.[100] For lighting elements, phosphor screen is printed on the inner surface of the glass and backed by a thin Al film (~100 nm) to give electrical conductivity. A lifetime test of the lighting element suggests a lifetime of over 10000 hours.[97]

18.6.5 Nanotube–Polymer Composites

Using nanotubes as reinforcing fibers in composite materials is still a developing field from both theoretical and experimental perspectives. Several experiments regarding the mechanical properties of nanotube–polymer composite materials with MWCNTs have been reported recently.[29–31,101] Wagner et al.[30] experimentally studied the fragmentation of MWNTs within thin polymeric films (urethane/diacrylate oligomer EBECRYL 4858) under compressive and tensile strain. They found that the nanotube–polymer interfacial shear stress τ is of the order of 500 MPa, which is much larger than that of conventional fibers with polymer matrix. This has suggested the possibility of chemical bonding between the nanotubes and the polymer in their composites, but the nature of the bonding is not clearly known. Lourie et al.[22] have studied the fragmentation of single-walled CNT within the epoxy resin under tensile stress. Their experiment also suggests a good bonding between the nanotube and the polymer in the sample. Schadler et al.[29] have studied the mechanical properties of 5 wt.% MWNTs within epoxy matrix by measuring the Raman peak shift when the composites are under compression or under tension. The tensile modulus of the composites, in this experiment, is found to enhance much less than the enhancement of the same composite under compression. This difference has been attributed to the sliding of inner shells of the MWNTs when a tensile stress was applied. In cases of SWNT polymer composites, the possible sliding of individual tubes in the SWCNT rope may also reduce the efficiency of load transfer. It is suggested that for the SWNT rope case, interlocking using polymer molecules might bond SWCNT rope more strongly. Andrews et al.[101] have also studied the composites of 5 wt.% of SWNT embedded in petroleum pitch matrix, and their measurements show an enhancement of the Young's modulus of the composite under tensile stress. Measurements by Qian et al.[31] of a 1 wt.% MWNT–polystyrene composite under tensile stress also show a 36% increase of Young's modulus compared with the pure polymer system. The possible sliding of inner shells in

MWCT and of individual tubes in an SWNT rope is not discussed in the above two studies. There are currently no clean experiments available on SWCNT–polymer composites, perhaps because SWCNTs are not available in large quantities for experimentation on bulk composite materials.

18.6.6 Other Applications

In addition to the fields discussed above, CNTs are being investigated for several other applications. The possibility to store hydrogen for fuel cell development has received much attention.[102] An H_2 storage capability of 8% by weight appears to be the target for use in automobiles. Though interesting basic science of hydrogen storage has been emerging, no technological breakthrough has been reported yet. Filling nanotubes with a variety of metals has also been attempted.[103–106] Most noteworthy of these attempts involves lithium storage for battery applications.[105,106] The thermal conductivity of SWCNTs is reported[107] to be about 3000 W/mK in the axial direction, which is second only to epitaxial diamond. This property can be exploited for cooling semiconductor chips and heat pipes. SWCNTs and MWCNTs are useful as high surface area and high-conductivity electrodes in a variety of applications. CNTs are being studied for gas absorption, for separation, and as support for catalysts. Other interesting applications include nanoscale reactors, ion channels, and drug delivery systems.

18.7 Concluding Remarks

Carbon nanotubes show remarkable potential in a wide variety of applications such as future nanoelectronics devices, field emission devices, high-strength composites, sensors, and in many related fields. This potential has propelled concentrated research activities across the world in growth, characterization, modeling, and application development. Though significant progress has been made in the last 5 years, numerous challenges remain; and there is still a great deal of work to be done before CNT-based products become ubiquitous. The biggest challenge now is to have control over the chirality and diameter during the growth process; in other words, the ability to specify *a priori* and obtain the desired chiral nanotubes is important to develop computing and related applications. Issues related to contacts, novel architectures, and development of inexpensive manufacturing processes are additional areas warranting serious consideration in electronics applications. The major roadblock now to developing structural applications is the lack of availability of raw materials in large quantities. With current bulk production rate of SWCNTs hovering around a few grams per hour, large-scale composite development efforts are nonexistent at present. This scenario will change with breakthroughs in large-scale production of CNTs, bringing the cost per pound to reasonable levels for structural applications. Sensor development efforts are in the early stages; numerous areas, such as functionalization, signal processing and integrity, and system integration, require significant further developments. In all of the above areas, modeling and simulation is expected to continue to play a critical role as it has been since the discovery of carbon nanotubes.

Acknowledgments

The authors thank the members of the experimental group at NASA Ames Research Center for Nanotechnology for their contributions to the material presented in this chapter, and we thank Harry Partridge for his critical review of the manuscript. Deepak Srivastava acknowledges support of his work by NASA contract 704–40–32 to CSC.

References

1. S. Iijima, *Nature*, 354, 56 (1991).
2. M.S. Dresselhouse, G. Dresselhouse, and P.C. Eklund, *Science of Fullerenes and Carbon Nanotubes,* Academic Press, New York, 1996.
3. D. Srivastava, M. Menon, and K. Cho, *Comp. Eng. Sci.,* 42 (2001).

4. M.S. Daw and M.I. Baskes, *Phys. Rev. Lett.* 50, 1285 (1983); S.M. Foiles, M.I. Baskes, and M.S. Daw, *Phys. Rev. B* 33, 7983 (1986).
5. F.H. Stillinger and T.A. Weber, *Phys. Rev. B* 31, 5262 (1985).
6. J. Tersoff, *Phys. Rev. B* 38, 9902 (1988).
7. D.W. Brenner, *Phys. Rev. B* 42, 9458 (1990).
8. B.J. Garrison and D. Srivastava, *Ann. Rev. Phys. Chem.* 46, 373 (1995).
9. D. Srivastava and S. Barnard, in *Proc. IEEE Supercomp. '97* (1997).
10. R. Car and M. Parrinello, *Phys. Rev. Lett.* 55, 2471 (1985).
11. W.A. Harrison, *Electronic Structure and the Properties of Solids*, Freeman, San Francisco, 1980.
12. M. Menon and K.R. Subbaswamy, *Phys. Rev. B* 55, 9231 (1997).
13. M. Menon, *J. Chem. Phys.*, 114, 7731 (2000).
14. Payne, M.C. et al., *Rev. Mod. Phys.* 68, 1045 (1992).
15. P. Hohenberg and W. Kohn, *Phys. Rev.* 136, 864B (1964).
16. W. Kohn and L.J. Sham, *Phys. Rev.* 140, 1133A (1965).
17. Details available at: http://cms.mpi.univie.ac.at/vasp/
18. See for example methodology and references in S.Datta, *Electronic Transport in Mesoscopic Systems*, Cambridge University Press, Cambridge, 1995.
19. B.I. Yakobson, C.J. Brabec, and J. Bernholc, *Phys. Rev. Lett.* 76, 2511 (1996).
20. D. Srivastava, M. Menon, and K. Cho, *Phys. Rev. Lett.* 83, 2973 (1999).
21. B.I.Yakobson and P. Avouris, *Mechanical Properties of Carbon Nanotubes*, M.S. Dresselhaus and P. Avouris (Eds.), Springer-Verlag, Berlin, 2001, p. 293.
22. O. Lourie, D.M. Cox, and H.D. Wagner, *Phys. Rev. Lett.* 81, 1638 (1998).
23. M.B. Nardelli, B.I. Yakobson, and J. Bernholc, *Phys. Rev. Lett.* 81, 4656 (1998).
24. P. Zhang and V. Crespi, *Phys. Rev. Lett.* 81, 5346 (1998).
25. C. Wei, D. Srivastava, and K. Cho, *Comp. Mod. Eng. Sci.,* 3, 255 (2002).
26. C. Wei, K. Cho, and D. Srivastava, *Phys. Rev. Lett.* submitted (2002).
27. M. Yu, O. Lourie, M. Dyer, K. Moloni, T. Kelly, and R. Ruoff, *Science* 287, 637 (2000).
28. B. Vigolo et al., *Science*, 290, 1331 (2000).
29. L.S. Schadler, S.C. Giannaris, and P.M. Ajayan, *Appl. Phys. Lett.* 73, 3842(1998).
30. H.D. Wagner, O. Lourie, Y. Feldman, and R. Tenne, *Appl. Phys. Lett.* 72, 188 (1998).
31. Q. Qian, E.C. Dickey, R. Andrews, and T. Rantell, *Appl. Phys. Lett.* 76, 2868 (2000).
32. C. Wei, D. Srivastava, and K. Cho, *Nano. Lett.,* 2, 647 (2002).
33. P. Collins and P. Avouris, *Sci. Am.* (Dec. 2000), p. 62.
34. L. Chico, V.H. Crespi, L.X. Benedict, S.G. Louie, and M.L. Cohen, *Phys. Rev. Lett.* 76, 971 (1996).
35. Z. Yao, H.W.C. Postma, L. Balants, and C. Dekker, *Nature* 402, 273 (1999).
36. M. Menon and D. Srivastava, *Phys. Rev. Lett.* 79, 4453 (1997).
37. T. Rueckes, K. Kim, E. Joselevich, G.Y. Tseng, C.-L. Cheung, and C.M. Lieber, *Science* 289, 94 (2000).
38. C. Joachim, J.K. Gimzewski, and A. Aviram, *Nature* 408, 541 (2000).
39. M. Menon and D. Srivastava, *J. Mater. Res.* 13, 2357 (1998).
40. C. Papadopoulos, A. Rakitin, J. Li, A.S. Vedeneev, and J.M. Xu, *Phys. Rev. Lett.* 85, 3476 (2000).
41. C. Satishkumar, P.J. Thomas, A. Govindraj, and C.N.R. Rao, *Appl. Phys. Lett.* 77, 2530 (2000).
42. A. Antonis, M. Menon, D. Srivastava, G. Froudakis. and L.A. Chernozatonskii, *Phys. Rev. Lett.* 87, 66802 (2001).
43. A. Antonis, M. Menon, D. Srivastava, and L.A. Chernozatonskii, *Appl. Phys. Lett.* 79, 266 (2001).
44. S.K. Moore, *IEEE Spectrum*, (Oct. 2000), pp. 18–19.
45. I.L. Chuang, L.M.K. Vandersypen, X.L. Zhou, D.W. Leung, and S. Lloyd, *Nature* 393, 143 (1998).
46. B.E. Kane, *Nature* 393, 133 (1998).
47. S. Park, D. Srivastava, and K. Cho, *J. Nanosci. Nanotechnol.*, 1, 75 (2001).
48. C. Knapp et. al., *Molec. Phys.* 95, 999 (1998).
49. F.J. Banhart and P.M. Ajayan, *Nature* 382, 433 (1996).

50. J. Kong, N.R. Franklin, C. Zhou, M.G. Chapline, S. Peng, K.J. Cho, and H. Dai, *Science* 287, 622 (2000).
51. S. Peng and K.J. Cho, *Nanotechnology* 11, 57 (2000).
52. D. Srivastava et al., *J. Phys. Chem. B* 103, 4330 (1999).
53. L. Yang and J. Han, *Phys. Rev. Lett*. 85, 154 (2000).
54. O. Gulseran, T. Yildirium, and S. Ciraci, *Phys. Rev. Lett.* 87, 116802 (2001).
55. S. Peng and K. Cho, *J. Appl. Mech.* in press (2002).
56. C. Montemagno and G. Bachand, *Nanotechnology* 10, 225 (1999).
57. J. Han, A. Globus, R. Jaffe, and G. Deardorff, *Nanotechnology* 8, 95 (1997).
58. D. Srivastava, *Nanotechnology* 8, 186 (1997).
59. C.H. Kiang, W.A. Goddard, R. Beyers, and D.S. Bethune, *Carbon*, 33, 903 (1995).
60. T. Guo, P. Nikolaev, A. Thess, D.T. Colbert, and R.E. Smalley, *Chem. Phys. Lett.* 243, 49 (1995).
61. H. Dai, A.G. Rinzler, P. Nikolaev, A. Thess, D.T. Colbert, and R.E. Smalley, *Chem. Phys. Lett.* 260, 471 (1996).
62. J. Kong, H.T. Soh, A.M. Cassell, C.F. Quate, and H. Dai, *Nature* 395, 878 (1998).
63. A.M. Cassell, S. Verma, J. Han, and M. Meyyappan, *Langmuir* 17, 260 (2001).
64. H. Kind, J.M. Bonard, L. Forro, K. Kern, K. Hernadi, L. Nilsson, and L. Schlapbach, *Langmuir* 16, 6877 (2000).
65. M. Su, B. Zheng, and J. Liu, *Chem. Phys. Lett*. 322, 321 (2000).
66. L. Delzeit, B. Chen, A. Cassell, R. Stevens, C. Nguyen, and M. Meyyappan, *Chem. Phys. Lett.* 348, 368 (2001).
67. H. Karzow and A. Ding, *Phys. Rev. B* 60, 11180 (1999).
68. Y.Y. Wei, G. Eres, V.I. Merkulov, and D.H. Lowndes, *Appl. Phys. Lett.* 78, 1394 (2001).
69. Y.C. Choi, Y.M. Shin, S.C. Lim, D.J. Bae, Y.H. Lee, B.S. Lee, and D.C. Chung, *J. Appl. Phys.* 88, 4898 (2000).
70. C. Bower, W. Zhu, S. Jin, and O. Zhou, *Appl. Phys. Lett.* 77, 830 (2000).
71. J. Li, C. Papadopoulos, J.M. Xu, and M. Moskovits, *Appl. Phys. Lett.* 75, 367 (1999).
72. B.C. Satishkumar, A. Govindraj, R. Sen, and C.N.R. Rao, *Chem. Phys. Lett.* 293, 47 (1998).
73. R. Andrews, D. Jacques, A.M. Rao, F. Derbyshire, D. Qian, X. Fan, E.C. Dickey, and J. Chen, *Chem. Phys. Lett.* 303, 467 (1999).
74. P. Nikolaev, M.J. Bronikowski, R.K. Bradley, F. Rohmund, D.T. Colbert, K.A. Smith, and R.E. Smalley, *Chem. Phys. Lett*. 313, 91 (1999).
75. J. Liu et al., *Science* 280, 1253 (1998).
76. B. Khare, M. Meyyappan, A.M. Cassell, C.V. Nguyen, and J. Han, *Nano Lett*. 2, 73 (2002).
77. A.M. Rao et al., *Science* 275, 187 (1997).
78. M.A. Pimenta et al., *Phys. Rev. B* 58, 16016 (1998).
79. A. Jorio et al., *Phys. Rev. Lett.* 86, 1118 (2001).
80. A.M. Rao et al., *Phys. Rev. Lett.* 84, 1820 (2000).
81. J. Chen et al., *Science* 282, 95 (1998).
82. E.T. Michelson et al., *Chem. Phys. Lett*. 296, 188 (1998).
83. S.S. Wang, J.D. Harper, P.T. Lansbury, and C.M. Lieber, *J. Am. Chem. Soc.* 120, 603 (1998).
84. H. Dai, N. Franklin, and J. Han, *Appl. Phys. Lett*. 73, 1508 (1998).
85. C.L. Cheung, J.H. Hafner, and C.M. Lieber, *Proc. Nat. Acad. Sci.* 97, 3809 (2000).
86. C.V. Nguyen, K.J. Cho, R.M.D. Stevens, L. Delzeit, A. Cassell, J. Han, and M. Meyyappan, *Nanotechnology* 12, 363 (2001).
87. S.J. Tans, A.R.M. Verschueren, and C. Dekker, *Nature* 393, 49 (1998).
88. R. Martel, T. Schmidt, H.R. Shea, T. Hertel, and P. Avouris, *Appl. Phys. Lett.* 2 73, 2447 (1998).
89. T. Yamada, *Appl. Phys. Lett.* 76, 628 (2000).
90. X. Liu, C. Lee, C. Zhou, and J. Han, *Appl. Phys. Lett.* 79, 3329 (2001).
91. A. Bachtold, P. Hadley, T. Nakanishi, and C. Dekker, *Science* 294, 1317 (2001).
92. H. Dai et al., *J. Phys. Chem. B* 103, 11246 (1999).

93. P.G. Collins, K. Bradley, M. Ishigami, and A. Zettl, *Science* 287, 1801 (2000).
94. J.M. Xu, *Infrared Phys. Tech*. 42, 485 (2001).
95. W.A. de Heer, A. Chatelain, and D. Ugarte, *Science* 270, 1179 (1995).
96. P.G. Collins and A. Zettl, *Appl. Phys. Lett.* 69, 1969 (1996).
97. Y. Saito, S. Uemura, and K. Hamaguchi, *Jpn. J. Appl. Phys. Part 2* 37, L 346 (1998).
98. X. Xu and G.R. Brandes, *Appl. Phys. Lett.* 74, 2549 (1999).
99. W. Zhu, C. Bower, O. Zhou, G. Kochanski, and S. Jin, *Appl. Phys. Lett.* 75, 873 (1999).
100. W.B. Choi, Y.H. Lee, D.S. Chung, N.S. Lee, and J.M. Kim, in D. Tomanek and R. Enbody (Eds.), *Science and Application of Nanotubes*, Kluwer Academic/Plenum Publishers, New York, 2000, p. 355.
101. R. Andrews et. al., *Appl. Phys. Lett.* 75, 1329 (1999).
102. Y. Ye et al., *Appl. Phys. Lett.* 304, 207 (1999).
103. M. Terroves et al., *MRS Bull*. p. 43, August 1999.
104. C. Kiang et al., *J. Phys. Chem. B* 103, 7449 (1999).
105. I. Mukhopadhyay et al., *J. Electrochem. Soc.* 149, A39 (2002).
106. J.S. Sakamoto and B. Dunn, *J. Electrochem. Soc.* 149, A26 (2002).
107. M.A. Osman and D. Srivastava, *Nanotechnology* 12, 21 (2001).